UCLA
UCLA Previously Published Works

Title

Response to Programmed Cell Death-1 Blockade in a Murine Melanoma Syngeneic Model Requires Costimulation, CD4, and CD8 T Cells

Authors

Moreno, Blanca Homet
Zaretsky, Jesse M
Garcia-Diaz, Angel
et al.

Cancer
Immunology
Research

2 Q1
3 Q2
4

Response to Programmed Cell Death-1 Blockade in a Murine Melanoma Syngeneic Model Requires Costimulation, CD4, and CD8 T Cells

5 AU Blanca Homet Moreno[1,2], Jesse M. Zaretsky[1,2], Angel Garcia-Diaz[1], Jennifer Tsoi[2],
6 Giulia Parisi[1], Lidia Robert[1], Katrina Meeth[3,4], Abibatou Ndoye[5], Marcus Bosenberg[3,4],
7 Ashani T. Weeraratna[5], Thomas G. Graeber[2,6], Begoña Comin-Anduix[6,7],
8 Siwen Hu-Lieskovan[1,6], and Antoni Ribas[1,2,6,7]

Abstract

The programmed cell death protein 1 (PD-1) limits effector T-cell functions in peripheral tissues, and its inhibition leads to clinical benefit in different cancers. To better understand how PD-1 blockade therapy modulates the tumor–host interactions, we evaluated three syngeneic murine tumor models, the $BRAF^{V600E}$-driven YUMM1.1 and YUMM2.1 melanomas, and the carcinogen-induced murine colon adenocarcinoma MC38. The YUMM cell lines were established from mice with melanocyte-specific $BRAF^{V600E}$ mutation and $PTEN$ loss ($BRAF^{V600E}/PTEN^{-/-}$). Anti–PD-1 or anti–PD-L1 therapy engendered strong antitumor activity against MC38 and YUMM2.1, but not YUMM1.1. PD-L1 expression did not differ between the three models at baseline or upon interferon stimulation. Whereas mutational load was high in MC38, it was lower in both YUMM models. In YUMM2.1, the antitumor activity of PD-1 blockade had a critical requirement for both CD4 and CD8 T cells, as well as CD28 and CD80/86 costimulation, with an increase in $CD11c^{+}$ $CD11b^{+}MHC-II^{high}$ dendritic cells and tumor-associated macrophages in the tumors after PD-1 blockade. Compared with YUMM1.1, YUMM2.1 exhibited a more inflammatory profile by RNA sequencing analysis, with an increase in expression from chemokine-trafficking genes that are related to immune cell recruitment and T-cell priming. In conclusion, response to PD-1 blockade therapy in tumor models requires CD4 and CD8 T cells and costimulation that is mediated by dendritic cells and macrophages. *Cancer Immunol Res; 4(10); 1–13. ©2016 AACR.*

Introduction

The development of inhibitors of the programmed cell death protein 1 (PD-1) or its ligand (PD-L1) represents a paradigm shift in the treatment of advanced cancers, with significant clinical benefits demonstrated in patients with several different histologies (1–4). Tumor responses are associated with a higher number of pretreatment PD-L1–expressing tumor and myeloid cells (5, 6), a high mutational load leading to increase in antigen-specific T-cell recognition (7, 8), the ability of PD-1/PD-L1 blockade to increase antigen presentation (9, 10) and modulate the tumor microenvironment (10, 11), and pre-existing CD8 T-cell infiltration (5, 12). A higher tumor mutational load induced by carcinogens such as ultraviolet light for melanoma (13) or cigarette smoking for lung carcinomas (14) would allow T cells to better differentiate between cancer and normal cells, thereby leading to immune recognition that could be unleashed by PD-1 blockade therapy.

Despite these advances, a better understanding is needed of the tumor–host interactions and how anti–PD-1 agents modulate cellular and molecular characteristics of each individual microenvironment. It is widely accepted that PD-1 blockade agents regulate T-cell activity in peripheral tissues in the context of infection or in tumors where PD-1/L1 checkpoint is the dominant inhibitory pathway. However, anti–PD-1 interacts earlier with T cells positively regulated by B7-CD28 costimulation (15), and this interaction is less well characterized (16–18).

In this study, we analyzed different tumor–host characteristics that might influence the effects of PD-1 blockade in murine models with a fully functional immune system. We conclude that T-cell priming and costimulation are required for anti–PD-1 therapy response to be effective in the melanoma tumor models *in vivo*.

Materials and Methods

Mice, cell lines, and reagents

C57BL/6 mice, B6.Cg-Braftm1MmcmPtentm1HwuTg(Tyr-cre/ERT2)13Bos/BosJ, B6.129S2-Cd28tm1Mak/J, and B6.129S4-

[1]Division of Hematology/Oncology, Department of Medicine, University of California (UCLA), Los Angeles, California. [2]Department of Molecular and Medical Pharmacology, UCLA, Los Angeles, California. [3]Departments of Immunobiology, Dermatology, and Pathology, Yale University School of Medicine, New Haven, Connecticut. [4]Howard Hughes Medical Institute, Chevy Chase, Maryland. [5]Melanoma Research Center, The Wistar Institute, Philadelphia, Pennsylvania. [6]Jonsson Comprehensive Cancer Center (JCCC) at UCLA, Los Angeles, California. [7]Division of Surgical Oncology, Department of Surgery, UCLA, Los Angeles, California.

Note: Supplementary data for this article are available at Cancer Immunology Research Online (http://cancerimmunolres.aacrjournals.org/).

Corresponding Authors: A. Ribas, University of California, Los Angeles, 10833 Le Conte Avenue, Los Angeles, CA 90095. Phone: 310-206-3928; Fax: 310-825-2493; E-mail: aribas@mednet.ucla.edu; or S. Hu-Lieskovan, Division of Hematology-Oncology, 11-934 Factor Building, 10833 Le Conte Avenue, Los Angeles, CA 90095-1782. Phone: 310-794-4955; Fax: 310-825-2493; E-mail: shu-lieskovan@mednet.ucla.edu

Cd80tm1Shr Cd86tm2Shr/J mice (Jackson Laboratories) were bred and kept under defined-flora pathogen-free conditions at the AALAC-approved animal facility of the Division of Experimental Radiation Oncology, UCLA, and used under the UCLA Animal Research Committee protocol #2004-159-23. Cell lines were cultured in DMEM media (Invitrogen) supplemented with 10% FBS (Omega Scientific) and 2 nmol/L L-glutamine (Invitrogen). YUMM1.1 and YUMM1.7 cell lines were obtained from induced tumors in conditional mouse models of melanoma based on melanocyte-specific $BRAF^{V600E}$ activating mutation and PTEN loss ($BRAF^{V600E}/PTEN^{-/-}$). YUMM2.1 was obtained from $BRAF^{V600E}/PTEN^{-/-}$ mice crossed with mice bearing a $Ctnnb1^{loxex3}$ allele (19), which targets exon 3, resulting in removal of the GSK3b kinase sites in β-catenin that are needed for ubiquitin-mediated destruction. However, analysis of the YUMM2.1 cell line showed that it had not recombined the β-catenin site (see below). YUMM cell lines were tested and authenticated by PCR and exome sequencing. Recombinant murine interferon gamma (IFNγ) was obtained from Peprotech. Tumors were followed by caliper measurement three times per week, and tumor volume was calculated using the following formula: tumor volume = $((width)^2 \times length)/2$. Mean and SD of the tumor volumes per group were calculated.

Antitumor studies in mouse models

To establish subcutaneous (s.c.) tumors, 3×10^5 MC38, 1×10^6 YUMM2.1, or 1×10^6 YUMM1.1 cells per mouse were injected into the flanks of C57BL/6 mice. When tumor diameter reached 4 to 5 mm, four doses of 300 μg of anti–PD-1 (Cat. No. BE0146, clone RMP1-14), anti–PD-L1 (Cat. No. BE0101, clone 10F.9G2), or isotype control antibody (Cat. No. BE0090, clone LTF-2), all from BioXCell, were injected intraperitoneally (i.p.) every 3 days. For T-cell subset depletion studies, 250 μg of anti-CD8 (Cat. No. BE0117, clone YTS 169.4), 250 μg of anti-CD4 (Cat. No. BE0003-2, clone OKT-4), both from BioXCell, or the combination were administered every 2 days starting the day before anti–PD-1 was initiated and through the duration of the experiment. For CD103 depletion, 200 μg of CD103 (Cat. No. BE0026, clone M290) from BioXCell was administered starting the day before anti–PD-1 treatment was initiated and administered i.p. every 2 days until the end of the experiment.

Whole-exome sequencing: Mutation calling and copy-number analysis

Sequencing of the MC38, YUMM2.1, YUMM1.7, and YUMM1.1 cell lines was performed to a mean depth of 55X, with >90% of targeted bases covered by more than 15 reads in all samples. Exonic mutations were annotated by the Ensembl Variant Effect Predictor (EVEP). MC38 was compared with tail DNA from a C57BL6 parental mouse, whereas the YUMM2.1 and YUMM1.1 were compared with tail DNA from a B6.Cg-Braftm1MmcmPtentm1HwuTg(Tyr-cre/ERT2)13Bos/BosJ mouse. Exon capture and library preparation were performed at the UCLA Clinical Microarray Core using the NimbleGenSeqCap EZ Mouse Exome Design Kit (Roche NimbleGen) targeting 54.3 megabases of genome. Note that 2 × 100 bp paired-end sequencing was carried out on the HiSeq 2000 platform (Illumina), and sequences were aligned to the UCSC mm10 reference (Burrows-Wheeler Aligner BWA-mem algorithm v0.7.9). Preprocessing followed the Genome Analysis Toolkit (GATK) Best Practices Workflow v3 (20), including

duplicate removal (Picard), indel realignment, and base quality score recalibration. Somatic mutations were called with methods modified from ref. 21 using Varscan2 (22), and the GATK-HaplotypeCaller. Mutations were annotated by EVEP release 80 (23) and filtered to remove those with a known database single-nucleotide polymorphism (dbSNP) reference SNP cluster identification to exclude residual strain-related differences due to imperfect backcross dilution. Depth ratio for copy-number variation was produced by Sequenza (24), with the ratio.priority option engaged.

RNA sequencing and enrichment analysis

RNA sequencing was performed using the Illumina HiSeq 2500 platform on 100-bp paired-end libraries prepared using the IlluminaTruSeq RNA sample preparation Kit. Reads were mapped using TopHat2 v2.0.9 (25) and aligned to the Musmusculus genome NCBI build 37.2. Reads were quantified and normalized using Cufflinks v2.2.1 (26) and CuffNorm to generate normalized expression tables by library size using the geometric normalization method. Resulting fragments per kilobase of exon per million fragments mapped expression values were log2 transformed with an offset of 1. To identify pathways enriched in the YUMM2.1 cell line, Gene Set Enrichment Analysis (GSEA) was performed using the preranked option. Genes were ranked by log_2 fold changes between YUMM2.1 and YUMM1.1 cell lines. Enrichment was assessed across the curated Molecular Signatures Database C5 GO biological process gene sets (27). RNA sequencing data have been deposited in GEO repository under the accession number GSE84264.

Flow cytometry analysis

MC38, YUMM2.1, and YUMM1.1 tumors and spleens were harvested from mice at predefined time points. Tumors were digested with collagenase D (Roche) and stained with antibodies to CD3 BV605, Ly6C FITC, PD-L1/CD274 PE, CD8a BV421, CD45RA/B220, CD11b BV785, CD11c PECy7, CD103 PerCP Cyanine 5.5, MHC Class II (I-A/I-E) FITC (Biolegend), Ly6G (Gr-1) PerCP Cyanine 5.5, F4/80 Pacific blue/eFluor450, CD25 APC, CD4 FITC (eBioscience). Intracellular staining of Foxp3 PE (eBioscience) was done according to the manufacturer's recommendations. Cells were analyzed with a LSR-II or FACSCalibur flow cytometer (BD Biosciences), followed by Flow-Jo software (Tree-Star) analysis (28).

Western blotting and immunofluorescence staining

Western blotting was performed using standard methods on lysates from cultured murine melanoma cell lines using primary antibodies to β-catenin, GAPDH and histone H3, and secondary anti-rabbit IgG horseradish peroxidase–linked antibody, all from Cell Signaling Technology, and Pdcd-1L1 (H-130) and gp100 (H-300) from Santa Cruz Biotechnology. Nuclear and cytoplasmic extraction reagents were obtained from Thermo Scientific. Proteins were visualized using ImageQuant 4000 scanner. Immunofluorescence staining was performed on tumor sections of frozen OCT blocks (Sakura Finetek) using primary antibodies to β-catenin (Cell Signaling Technology) and CD8a (BD Biosciences) followed by normal donkey serum and rat IgG(H+L) FITC-conjugated secondary antibody (Jackson Immunoresearch Laboratories; ref. 29).

Topflash analysis

Topflash vectors were obtained from Addgene (M51 Super 8x FOPFlash/TOPFlash mutant, Cat. No. 12457; M50 Super 8x TOPFlash, Cat. No. 12456). YUMM1.7 and YUMM2.1 cells (±10 µmol/L tamoxifen) were plated to achieve 70% confluency in 6-well plates. Cells were cotransfected with pTK-RLuc (green Renilla luciferase) along with either Topflash or Fopflash vectors. After 48 hours, cells were harvested and luciferase activity was measured using Dual-Luciferase Reporter Assay System (Cat. No. E1910) from Promega, where firefly luciferase signal was normalized to its corresponding Renilla luciferase signal. Topflash/fopflash signal was determined from each treatment and graphed using Graphpad/Prism.

β-Catenin downregulation

β-catenin shRNA lentiviral vector (Cat. No. 29210-V) and the negative control shRNA lentiviral vector (Cat. No. 108080) were purchased from Santa Cruz Biotechnology. YUMM2.1 and YUMM1.1 cells were transduced at a multiplicity of infection of 1 to 10 in media containing 5 µg/mL polybrene and then selected in complete DMEM with 2.5 µg/mL of puromycin for 3 weeks.

Statistical analysis

Data were analyzed with GraphPad Prism (version 5) software (GraphPad Software). Descriptive statistics such as number of observations, mean values, and SD were reported and presented graphically for quantitative measurements. Normality assumption was checked for outcomes before statistical testing. For measurements such as tumor volume or percentage of tumor-infiltrating lymphocytes (TIL), pairwise comparisons between treatment groups were performed by unpaired t tests. All hypothesis testing was two-sided, and a significance threshold of 0.05 for P value was used.

Results

In vivo syngeneic animal models with differential responses to PD-1 pathway blockade

In order to have animal models that consistently respond to anti–PD-1 therapy, we tested four melanoma models, three derived from $BRAF^{V600E}/PTEN^{-/-}$ genetically engineered mice (Supplementary Fig. S1A) and B16, and compared them with MC38, a cell line that has been previously shown to respond well to PD-1 blockade therapy (30, 31). In three replicate studies, we observed antitumor activity of anti–PD-1 or anti–PD-L1 antibody therapy against MC38 (Fig. 1A) and YUMM2.1 (Fig. 1B), but no antitumor activity against YUMM1.1 (Fig. 1C), YUMM1.7, or B16 (Supplementary Fig. S1B). Of note, these responses to anti–PD-1 antibody are incomplete, and both MC38 and YUMM2.1 tumors start regrowing around days 35 to 40 after tumor injection. We decided to focus our further mechanistic studies in MC38 for a tumor that is known to respond to anti–PD-1, and studied the differential responses in YUMM1.1 and YUMM2.1.

Similar PD-L1 expression induced in MC38, YUMM2.1, and YUMM1.1 by IFNγ

In order to investigate the mechanism of response to anti–PD-1 therapy, we first focused on induced PD-L1 expression in these three cell lines. Total cellular PD-L1 increased upon exposure to IFNγ in the three cell lines, with a higher magnitude of increase in MC38 cells than in YUMM2.1 and YUMM1.1 cells (Fig. 2A).

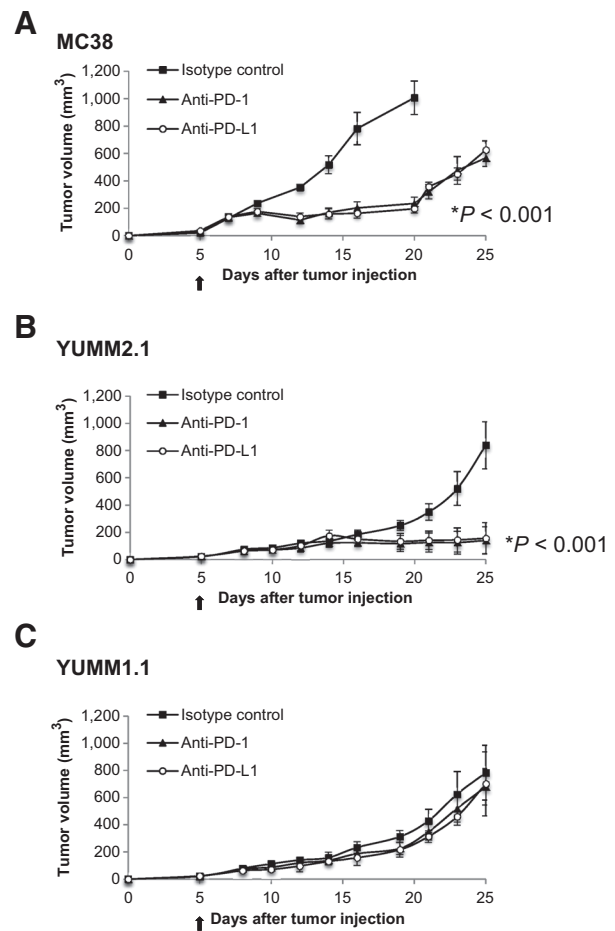**Figure. 1.**

Enhanced *in vivo* antitumor activity with anti–PD-1 or anti–PD-L1 in MC38 and YUMM2.1 tumor models compared with YUMM1.1. Tumor growth curves of MC38 **(A)**, YUMM2.1 **(B),** and YUMM1.1 **C**, with 4 mice in each group (mean ± SD) after anti–PD-1, anti–PD-L1, or isotype control. The arrow indicates the day when treatment with anti–PD-1, anti–PD-L1, or isotype control was started. *, $P < 0.001$ by unpaired t test on day 20, anti–PD-1 versus isotype control, anti–PD-L1 versus isotype control in MC38, anti–PD-1 versus isotype control, anti–PD-L1 versus isotype control in YUMM2.1 tumors.

Q10

Surface expression of PD-L1 was low at baseline, and increased upon exposure to IFNγ in the three cell lines, though less evident in the morphologically more heterogeneous YUMM1.1 cell line (Fig. 2B).

Increased mutational load in MC38 compared with YUMM1.1 and YUMM2.1

Next, we determined whether mutational load is a contributor to the observed differential response to anti–PD-1 therapy. MC38, which was established from a mouse exposed to the carcinogen dimethylhydralazine (32), has a higher mutational load (2,778 mutations), compared with the much lower mutational rates in YUMM1.1 and YUMM2.1 (128 and 68 nonsynonymous variants, respectively; Supplementary Fig. S1C). Despite independent derivation, 26 variants are shared by YUMM1.1 and YUMM2.1, which likely represent SNPs not found in the sequenced strain-matched control or in the National Center for Biotechnology
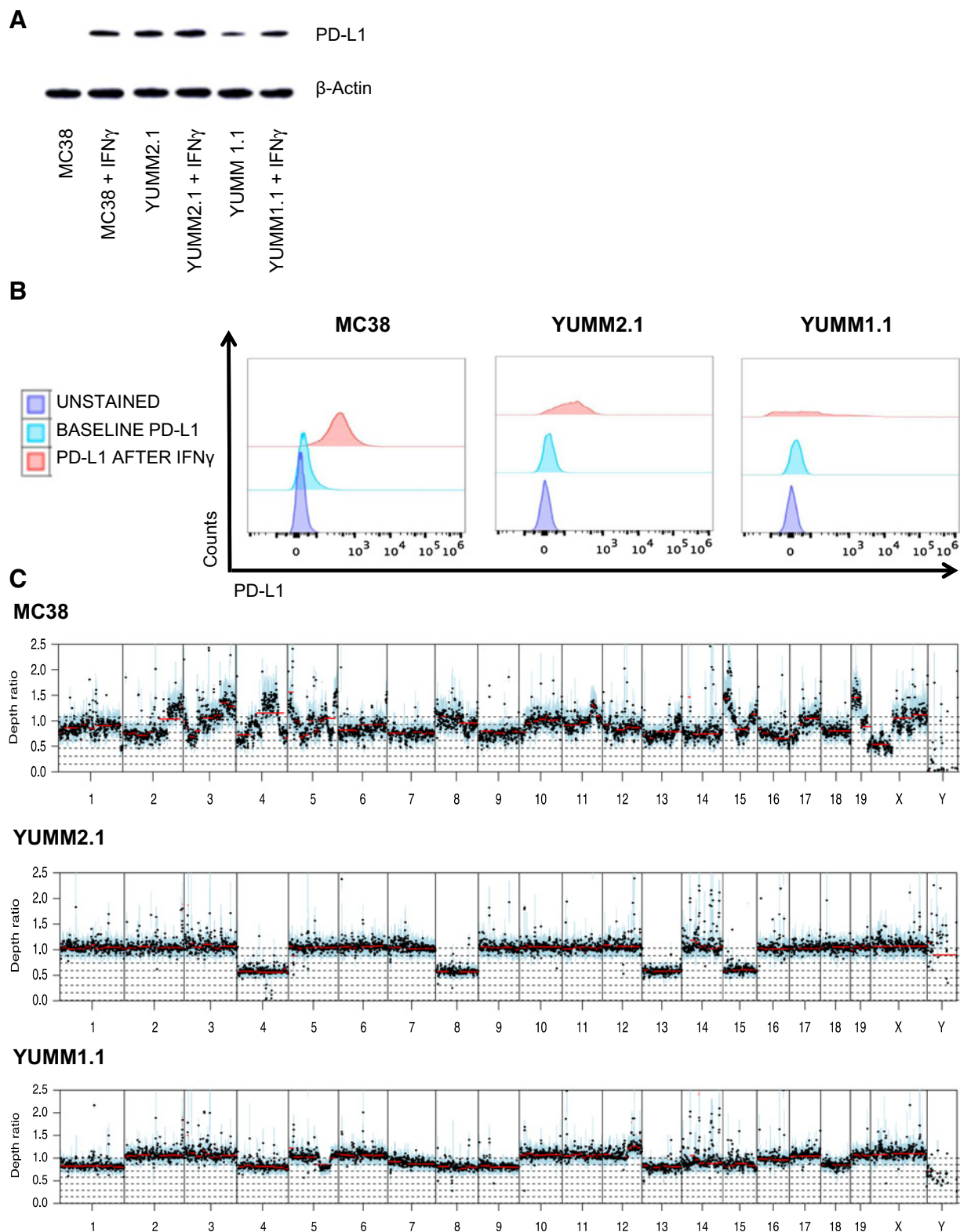
Figure 2.
IFNγ modulates PD-L1 expression in MC38, YUMM2.1, and YUMM1.1. **A,** Western blot analysis of PD-L1. MC38, YUMM2.1, and YUMM1.1 cells were cultured with or without IFNγ for 24 hours. **B,** expression of PD-L1 by flow cytometry on MC38, YUMM2.1, and YUMM1.1 cells at baseline and after 24 hours of stimulation with IFNγ. **C,** chromosomal copy-number variation in MC38, YUMM2.1, and YUMM1.1 cell lines. Y-axis represents Log$_2$ depth ratio vs. matched normal.
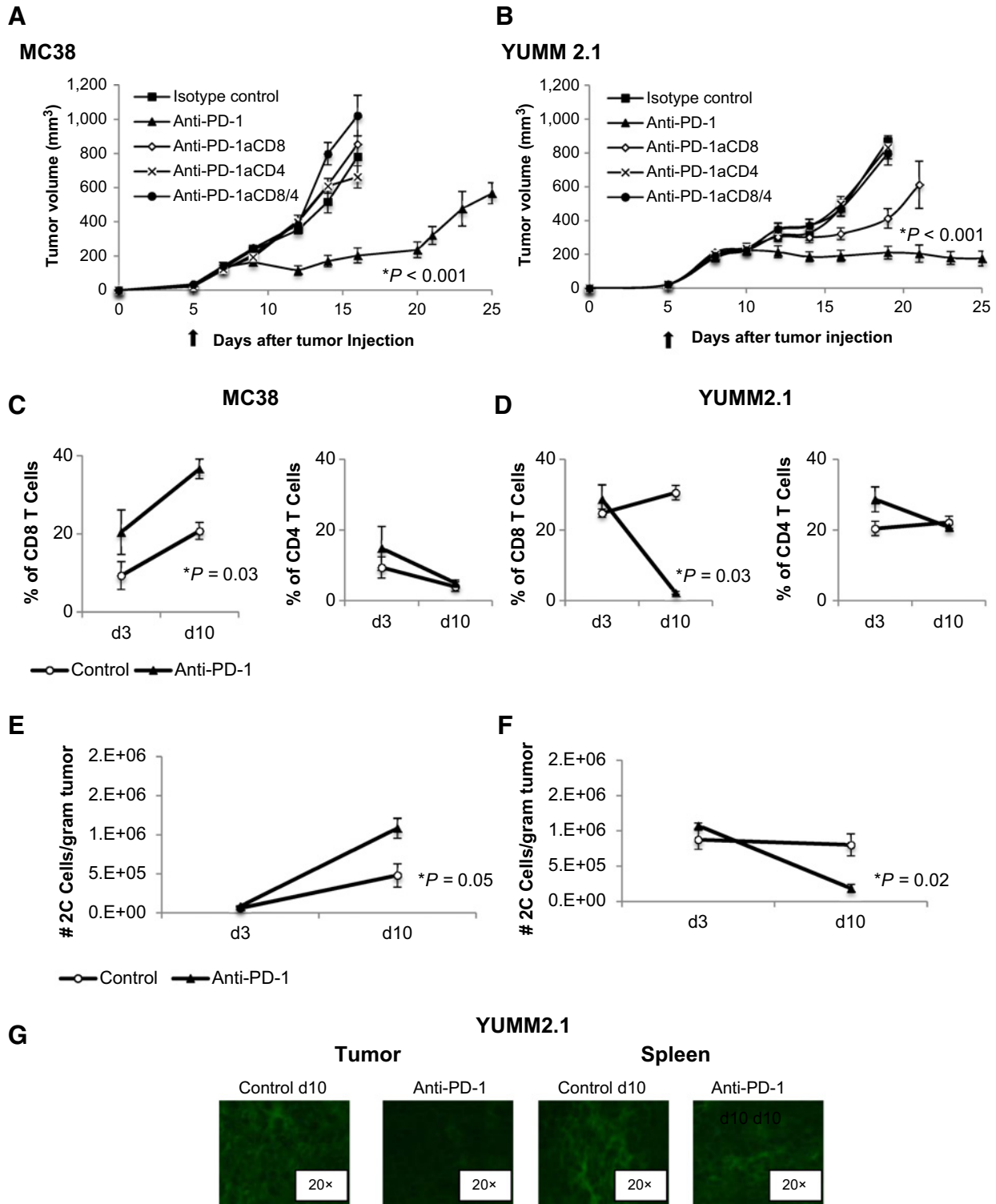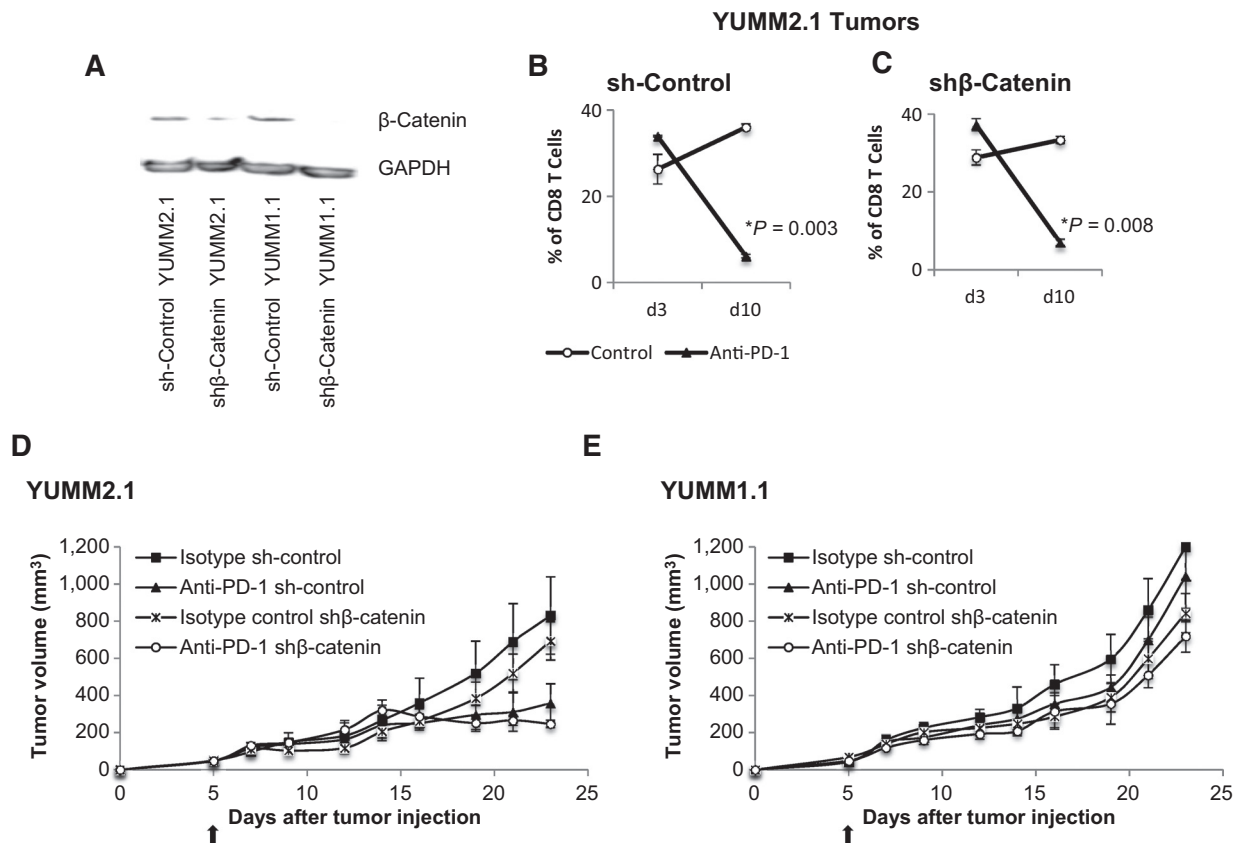
Figure 3.
Both CD8 and CD4 cells mediate response to PD-1 blockade in MC38 and YUMM2.1. Tumor growth curves of MC38 **(A)** and YUMM2.1 **(B)** after anti–PD-1 and either anti-CD8 (anti–PD-1aCD8), anti-CD4 (anti–PD-1aCD4), anti-CD8 + anti-CD4 (anti–PD-1aCD8/4) or isotype control; 4 mice in each group, mean ± SD.
(*, $P < 0.001$ isotype control, anti–PD-1aCD8, anti–PD-1aCD4, anti–PD-1aCD8/4 versus anti–PD-1 in MC38, $P < 0.001$ isotype control, anti–PD-1aCD4, anti–PD-1aCD8/4 versus anti–PD-1 in YUMM2.1, unpaired t test, $n = 4$); *, $P = 0.003$ anti–PD-1aCD8 versus anti–PD-1, unpaired t test, $n = 4$. The arrow indicates the day treatment with anti–PD-1 or isotype control was started. This experiment was performed in triplicate. (*Continued on the following page*)

Information database of genetic variation. Copy-number variation analysis revealed substantial differences in chromosomal alteration patterns between the three cell lines (Fig. 2C). However, most are shallow amplifications or deletions ($\log_2$ ratio between 0.5 and 1.5).

CD8 and CD4 T cells important in response to PD-1 blockade in MC38 and YUMM2.1

To elucidate the role of CD8 and CD4 T cells in anti–PD-1 activity, both cell subtypes were depleted in C57BL/6 mice bearing MC38 or YUMM2.1 tumors. Antibody-mediated depletion was confirmed in YUMM2.1 tumors and spleens (Supplementary Fig. S2A and S2B). In the absence of CD8 cells, CD4 cells, or both, antitumor response diminished in both MC38 and YUMM2.1 models (Fig. 3A and B). Of note, CD8 cell depletion (anti–PD-1aCD8) in the YUMM2.1 tumor model only partially abrogated the response to anti–PD-1 therapy, whereas CD4 cell depletion, or CD4 plus CD8 depletion, completely abrogated this response (Fig. 3B).

Increased TILs in MC38, but decreased in YUMM2.1, upon PD-1 blockade

Three and ten days after starting treatment with anti–PD-1 or isotype control, tumors and spleens were harvested and stained for CD3, CD4, and CD8 (Supplementary Fig. S2C and S2D). CD8 T-cell infiltration increased in MC38 tumors (calculated as percentage of all cells in the tumor) on day 3 and day 10 of treatment with anti–PD-1 when compared with isotype control (Fig. 3C), whereas CD8 T cells in the corresponding spleens of MC38 tumor–bearing mice remained unchanged (Supplementary Fig. S2E). No significant difference in the percentage of CD4 T cells was observed in MC38 tumors (Fig. 3C) and spleens (Supplementary Fig. S2F). However, CD8 T-cell infiltration into YUMM2.1 tumors was significantly decreased on day 10 of anti–PD-1 therapy when compared with isotype control. This decrease in CD8 T cells was not present on day 3 (anti–PD-1 d3) compared with isotype control group (Fig. 3D). CD8 T cells did not decrease in the corresponding spleens of any of the conditions in the YUMM2.1 model (Supplementary Fig. S2E). The percentage of CD4 T cells in the YUMM2.1 tumors or spleens was not significantly different across different time points or between anti–PD-1 and isotype control tumors (Fig. 3D). The YUMM1.1 tumor model did not show any CD8 T-cell variation in either tumors or spleens comparing anti–PD-1 and isotype control–treated conditions (Supplementary Fig. S2G). When we calculated the absolute number of CD8 T cells per gram of tumor pooled from two separate experiments, it confirmed the significant increase in CD8 T cells in the MC38 tumors (Fig. 3E) and the significant decrease in CD8 T cells in the YUMM2.1 tumors on day 10 of anti–PD-1 treatment (Fig. 3F). Immunofluorescence staining of tumors and spleens from mice in the YUMM2.1 group collected after anti–PD-1 therapy or isotype control also demonstrated a remarkable decrease in intratumoral CD8 T cells on day 10 and no change in spleen (Fig. 3G).

Wnt/β-catenin uninvolved in YUMM2.1 CD8 T-cell decrease or response to anti–PD-1

YUMM2.1 cell line was derived from a mouse with the same genetic background as YUMM1.1 but containing an additional transgenic allele that, when recombined by tamoxifen induction, produces a stabilized β-catenin, which leads to increased metastatic potential of the tumors (33). However, whole-exome sequencing and PCR showed that β-catenin was unrecombined in the YUMM2.1 cell line, and the recombination could be induced by tamoxifen (4HT; Supplementary Fig. S3A and S3B). Nevertheless, we observed that YUMM2.1 cells do have more β-catenin protein expression with increased activity tested in vitro (Supplementary Fig. S3C) and in macro-dissected tumor sections when implanted in mice (Supplementary Fig. S3D). Active Wnt/β-catenin was linked to T-cell exclusion in tumors (34). To test if β-catenin had a role in the immunogenicity of YUMM2.1 and the loss of CD8 infiltrates on day 10 after anti–PD-1 therapy, β-catenin in both YUMM2.1 and YUMM1.1 cell lines was knocked down and confirmed at the protein level (Fig. 4A). Knockdown of β-catenin in YUMM2.1 did not change the significant decrease of CD8 T cells on day 10 with anti–PD-1 treatment when compared with the respective isotype-treated controls (Fig. 4B and C). Silencing β-catenin did not change the antitumor response in the YUMM2.1 model (Fig. 4D), nor did it change in the nonresponsive YUMM1.1 model (Fig. 4E).

Requirement of costimulation with PD-1 blockade in YUMM2.1

The evidence that both CD4 and CD8 cells are required for response to PD-1 blockade in the MC38 and YUMM2.1 models suggests that T-cell priming and CD4 helper function may be needed to induce the cytotoxic response to the tumors, which was further studied. The antitumor activity of PD-1 blockade against YUMM2.1 was completely abolished in CD28 knockout (KO; Fig. 5A) and CD80/CD86 double KO mice (Fig. 5B), clearly demonstrating that costimulation is a requirement for the efficacy of anti–PD-1 blockade in this model.

Increased antigen-presenting dendritic cells in anti–PD-1-treated YUMM2.1 tumors

The next step was to identify the cells involved in antigen presentation and costimulation. We phenotyped the different subtypes of dendritic cells (DC) by staining for CD11c$^+$B220$^-$ (conventional) and CD11c$^+$B220$^+$ (plasmacytoid) subsets. Conventional DCs can be further subdivided into CD11c$^+$B220$^-$CD8$^+$ DCs, which are CD103$^+$ in peripheral tissues and have been reported to mediate antigen cross-presentation to CD8 T cells (35), and CD11c$^+$CD11b$^+$MHC-II^{high} DCs, which are considered to be dedicated APCs that present peptides on MHC-II molecules to CD4 T cells (ref. 36; gating strategy in Supplementary Fig. S4A and S4B). The percentage of CD11c$^+$B220$^-$ cells was significantly decreased in MC38 tumors of mice treated with anti–PD-1 compared with isotype control, with no significant change in YUMM2.1 or YUMM1.1 tumors (Fig. 5C).

(Continued.) On days 3 (d3) and 10 (d10) after treatment with anti–PD-1 or isotype control was started, MC38 and YUMM2.1 tumors were isolated and stained with fluorescent-labeled antibodies, analyzed by FACS. **C** and **D,** percentage of CD3$^+$CD8$^+$ (CD8 T cells) and CD3$^+$CD4$^+$ (CD4 T cells) in MC38 **(C)** and YUMM2.1. **D,** tumors are shown (mean ± SD). *, $P = 0.03$ anti–PD-1 d10 versus control d10 in MC38; $P = 0.03$ anti–PD-1 d10 versus control d10 in YUMM2.1 (unpaired t test, $n = 4$). Results were consistent in 6 replicate experiments. **E** and **F,** statistical analysis of the 2C total number of CD8 T cells per gram of tumor in MC38 **(E)** and **(F)** YUMM2.1 tumors. *, $P = 0.05$ anti–PD-1 d10 versus control d10 in MC38, $P = 0.02$ anti–PD-1 d10 versus control d10 in YUMM2.1, unpaired t test, $n = 8$). **G,** representative immunofluorescence of CD8 T cells stained in YUMM2.1 tumors and spleens d10 after treatment with anti–PD-1 or isotype control was started.

Figure 4.
Wnt/β-catenin pathway is not involved in CD8 T-cell decrease or anti–PD-1 antitumor response in YUMM2.1 tumor model. **A,** Western blot analysis of β-catenin in YUMM2.1 cells transduced with shRNA without β-catenin (sh YUMM2.1) or with shβ-catenin (shβ-catenin YUMM2.1) and YUMM1.1 cells transduced with shRNA without β-catenin (sh YUMM1.1) or with shβ-catenin (shβ-catenin YUMM1.1). **B,** quantification of CD3$^+$CD8$^+$ (CD8 T cells). Tumor cells harvested on days 3 and 10 after anti–PD-1 or isotype control were counted and analyzed by flow cytometry for CD3/CD8 staining; 3 mice in each group (mean ± SD). *, P = 0.003 anti–PD-1 d10 versus control d10 in sh-control YUMM2.1 tumors. **C,** shβ-catenin YUMM2.1 tumors. *, P = 0.008 anti–PD-1 d10 versus control d10 in shβ-catenin YUMM2.1 tumors, unpaired t test, n = 4. **(D)** in vivo sh and shβ-catenin YUMM2.1 and **(E)** sh and shβ-catenin YUMM1.1 tumor growth curves with 3 to 4 mice in each group (mean ± SD) after anti–PD-1 or isotype control.

The percentage of intratumoral CD11c$^+$B220$^-$CD8$^+$ and CD11c$^+$ B220$^-$CD103$^+$ DCs in MC38, YUMM2.1, or YUMM1.1 was not significantly different across time points or with PD-1 blockade therapy. A very small percentage of CD11c$^+$B220$^-$CD8$^+$ cells in YUMM2.1 tumors were present (Fig. 5D). Growth of tumors in mice that were CD103-depleted was analogous to nondepleted mice, with or without the addition of anti–PD-1 (Fig. 5E). Of note, anti–PD-1-treated YUMM2.1 tumors exhibited a significant increase in CD11c$^+$CD11b$^+$ and CD11c$^+$CD11b$^+$MHC-II^{high} DCs compared with isotype control–treated tumors (Fig. 5F). This finding was not present in MC38 tumors.

Increased tumor-associated macrophages in YUMM2.1 tumors treated with anti–PD-1

Another immune cell subtype potentially implicated in T-cell priming are tumor-associated macrophages (TAM). CD11b$^+$F4/ 80$^+$ TAMs were gated after the exclusion of dead cells (Supplementary Fig. S4C). The total percentage of TAMs decreased (not statistically significant) in MC38 tumors treated with anti–PD-1 (Fig. 6A). In contrast, TAMs significantly increased in YUMM2.1 tumors on day 10 after anti–PD-1 treatment was started. Immune-

suppressive TAMs (CD11b$^+$F4/80$^+$MHC-II^{low}, M2 TAMs) were more frequent in YUMM2.1 tumors with or without anti–PD-1 therapy, with an increase in the percentage of both CD11b$^+$F4/ 80$^+$MHC-II^{high} TAMs (M1 TAMs) and M2 TAMs upon PD-1 blockade (Fig. 6B). These observations were not present in YUMM1.1 tumors, where TAMs remained mostly unchanged (Fig. 6B). Taken together, TAMs may play a different role in YUMM2.1 tumors compared with MC38, although both tumor models respond to anti–PD-1 blockade.

No change in MDSCs or regulatory T cells with PD-1 blockade therapy

To evaluate the effect of anti–PD-1 on other cellular components of the tumor microenvironment, we harvested tumors 10 days after anti–PD-1 treatment was started and analyzed the two main subsets of myeloid-derived suppressor cells (MDSC): monocytic MDSCs (MO-MDSC, CD11b$^+$Ly6C^{high}Ly6G^{low}) and polymorphonuclear MDSCs (PMN-MDSC, CD11b$^+$Ly6C^{low}Ly6-G^{high}; Supplementary Fig. S4D). Anti–PD-1 did not change the percentage of MO-MDSCs or PMN-MDSC in any tumors compared with isotype control (Fig. 6C). Another
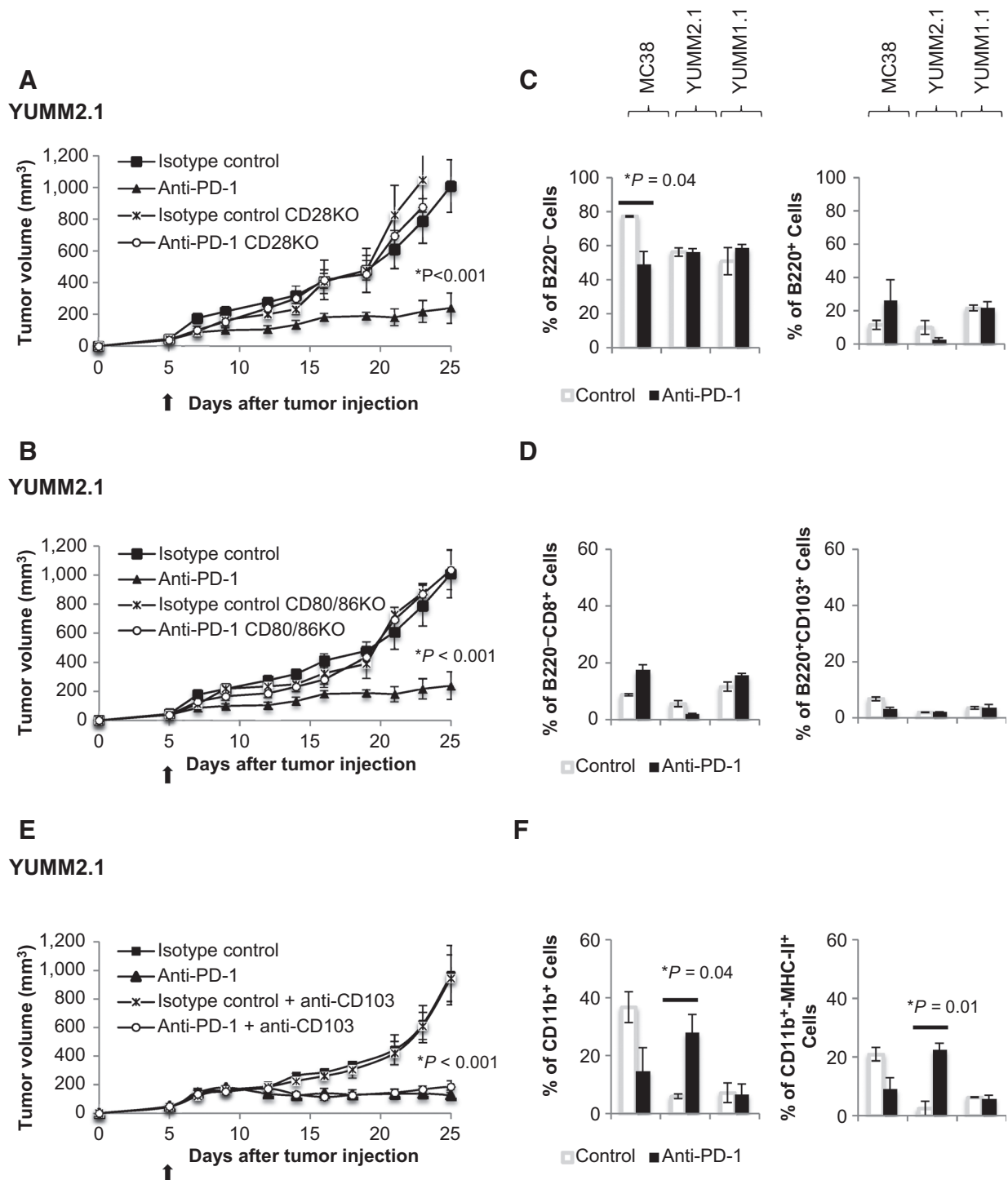
Figure 5.
Increased antigen-presenting DCs in anti–PD-1-treated YUMM2.1 tumors. **A,** tumor growth curves of CD28KO or C57BL/6 mice bearing YUMM2.1 treated with anti–PD-1 or isotype control. **B,** tumor growth curves of CD80/86KO or C57BL/6 mice bearing YUMM2.1 treated with anti–PD-1 or isotype control. Four mice in each group (mean ± SD). The arrow indicates the day treatment with anti–PD-1 or isotype control was initiated. **C,** on day 10 after starting treatment, MC38, YUMM2.1, and YUMM1.1 tumors were isolated and stained with fluorescent-labeled antibodies and analyzed by FACS, with 3 mice in each group (mean ± SD). B220$^-$ and B220$^+$ cells presented as percentage of CD11c$^+$ cells. *, $P = 0.04$ anti–PD-1 versus isotype control, CD11c$^+$B220$^-$ cells in MC38 tumors, unpaired t test, $n = 3$. **D,** B220$^-$CD8$^+$ and B220$^-$CD103$^+$ presented as percentage of CD11c$^+$ cells. **E,** *in vivo* YUMM2.1 growth curve after anti–PD-1 ± anti-CD103 or isotype control ± anti-CD103, 4 mice in each group (mean ± SD). The arrow indicates the day anti–PD-1 or isotype control treatment was started. **F,** CD11b$^+$ and CD11b$^+$MHC-II^{high} DCs presented as percentage of CD11c$^+$ cells. *, $P = 0.04$ anti–PD-1 versus control, $P = 0.01$ anti–PD-1 versus control in YUMM2.1 tumors, unpaired t test, $n = 3$.
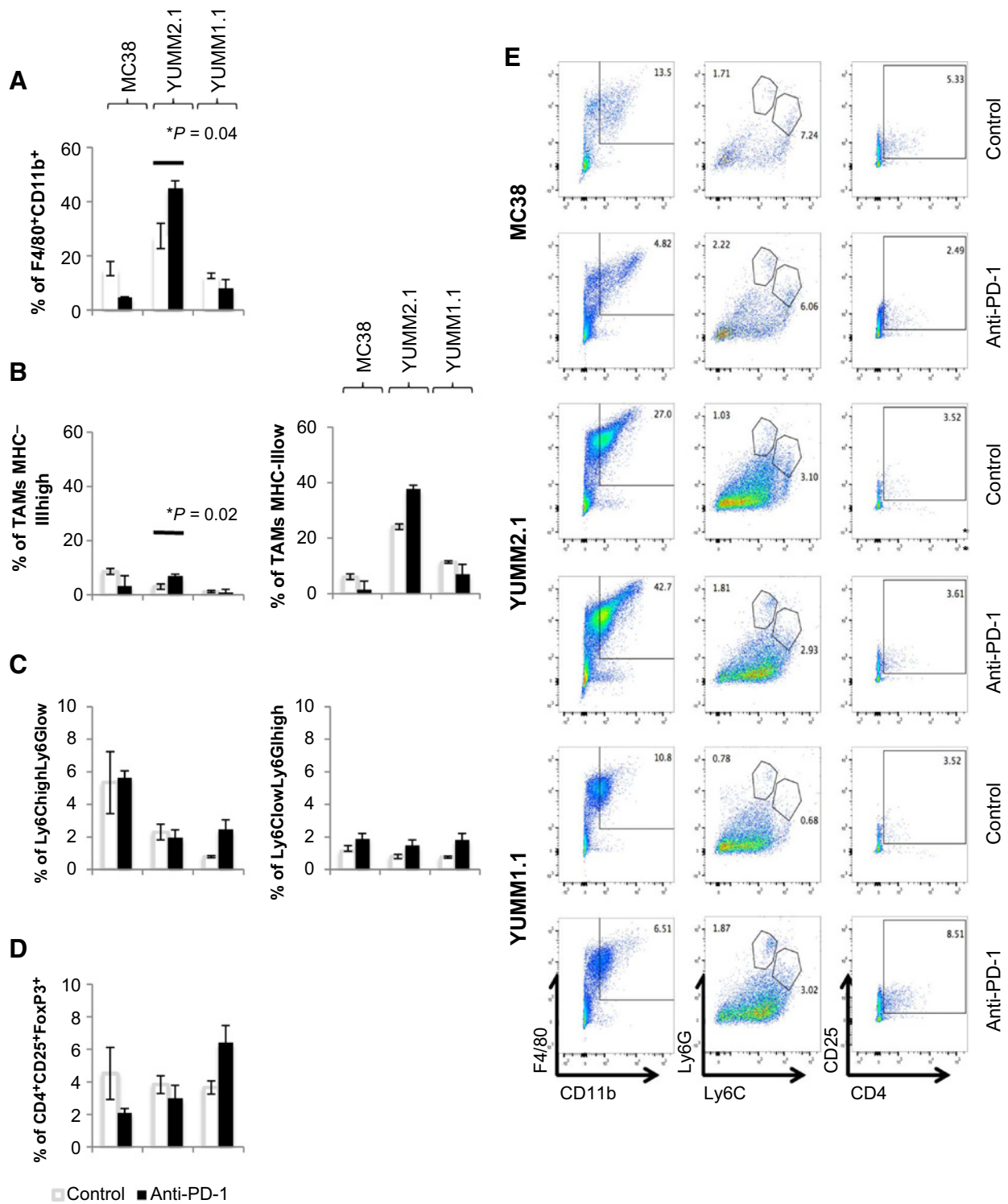
Figure 6.
Modulation of the tumor microenvironment by anti–PD-1 in MC38, YUMM2.1, and YUMM1.1. On day 10 after anti–PD-1 or isotype control, MC38, YUMM2.1, and YUMM1.1 tumors were isolated and stained with fluorescent-labeled antibodies and analyzed by FACS, with 3 mice in each group (mean ± SD). **A,** analysis of TAMs (CD11b$^+$F4/80$^+$). **B,** TAMs MHC-II^{high} (M1 TAMs, CD11b$^+$F4/80$^+$MHC-II^{high}) and TAMs MHC-II^{low} (M2 TAMs, CD11b$^+$F4/80$^+$MHC-II^{low}). *, $P = 0.04$ anti–PD-1 d10 versus control d10 TAMs; $P = 0.02$ anti–PD-1 d10 versus control d10 TAMs MHC-II^{high} in YUMM2.1 tumors, unpaired t test, $n = 3$. **C,** MO-MDSC (CD11b$^+$Ly6C^{high}Ly6G^{low}) and PMN-MDSC (CD11b$^+$Ly6C^{low}Ly6G^{high}) presented as percentage of CD11b$^+$ cells. **D,** analysis of T$_{regs}$ (CD4$^+$CD25$^+$FOXp3$^+$). **E,** representative FACS plots in tumors.

immune-suppressive cell population, regulatory T cells (T$_{regs}$; Supplementary Fig. S4E; T$_{regs}$, CD4$^+$CD25$^+$FOXp3$^+$), showed a nonstatistically significant trends toward a decrease in MC38 and YUMM2.1 tumors with anti–PD-1 and an increase in YUMM1.1 (Fig. 6D). Representative flow charts of TAMs, MDSCs, and T$_{regs}$ are shown in Fig. 6E.

A more inflammatory gene signature profile in YUMM2.1 compared with YUMM 1.1

RNA was extracted from cultured YUMM1.1 and YUMM2.1 and subjected to RNA sequencing. GSEA and pathway analyses indicated that immune response, cytokine production, and inflammatory-related genes were strongly represented in YUMM2.1 compared with YUMM = 1.1 cells (Fig. 7A). Corresponding normalized enrichment scores (NES), P values, and FDR of the GSEA plots are included (Fig. 7B). Analysis of genes that code for secreted proteins with a log$_2$-fold higher than 1 in YUMM2.1 compared with YUMM1.1 cells revealed an increase in inflammatory and chemotaxis-related genes (Supplementary Fig. S4F).

Discussion

Immunological checkpoint blockade with anti–PD-1 or anti–PD-L1 antibodies reverses cancer immunosuppression and promotes antitumor immune responses in several cancer types. Long-term responses with minimal side effects have been reported in patients with melanoma, lung, liver, kidney, bladder, mismatch repair–deficient colon cancers, and hematologic malignancies, among others (1–4, 31). Why these agents exhibit antitumor responses in certain histologies and only in a percentage of patients with the same type of tumor remains unknown. Here, we studied tumor models that respond differently to anti–PD-1 treatment and tested the reasons for anti–PD-1 activity in MC38 and YUMM2.1 tumors.

Upregulation of PD-L1 and its ligation to PD-1 on activated T cells is a well-described mechanism by which cancer tissues limit the host immune response, termed adaptive immune resistance (37). High baseline PD-L1–expressing tumor cells have been positively correlated with response to PD-1 blockade in patient samples (5, 6). However, PD-L1 was markedly increased upon IFNγ exposure in the three murine cell lines studied, which does not provide an explanation for the different responses to anti–PD-1.

Mutational load has been associated with a higher clinical benefit to immunotherapy (38–40). A greatly increased number of somatic mutations were observed in MC38 compared with YUMM2.1 and YUMM1.1, accompanied by high copy-number variation, consistent with its origin as a carcinogen-induced cell
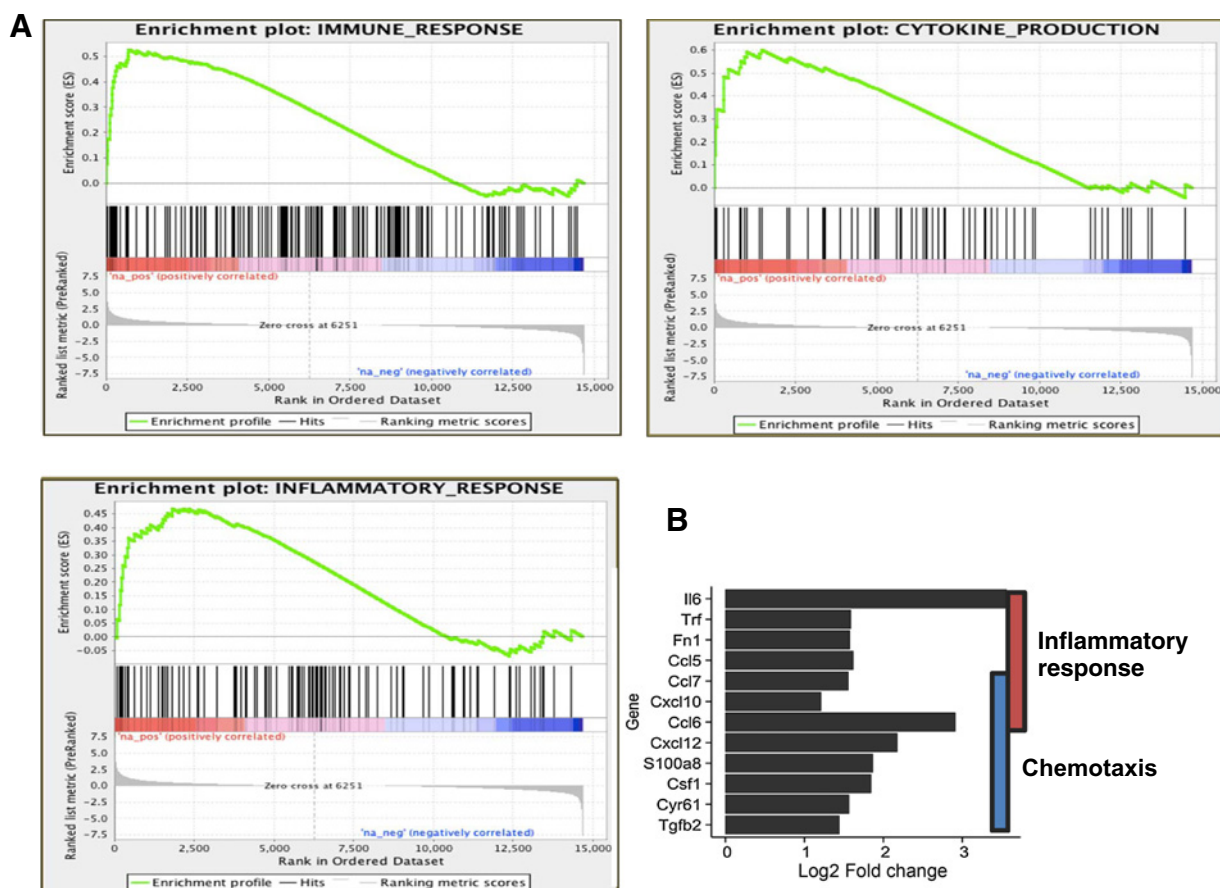

Figure 7.
YUMM2.1 is more inherently immune permissive than YUMM1.1. **A,** GSEA curves for YUMM2.1 versus YUMM1.1 enriched pathways involved in immune response, cytokine production, and inflammatory response. **B,** corresponding NES, P values, and FDR of the GSEA plots.

line. The high mutational load could be at least partially responsible for the effectiveness of anti–PD-1 therapy in MC38 tumors. However, both YUMM2.1 and YUMM1.1 displayed a very low number of new somatic mutations, consistent with tumors arising from genetically engineered mice driven by a strong driver oncogene and avoidance of senescence.

T-cell response has been widely accepted to be crucial for effective anti–PD-1/PD-L1 antitumor activity (41). We confirmed the essential roles of both the CD8 and CD4 T cells in anti–PD-1 effect in both MC38 and YUMM2.1 tumor models. Depletion of CD8 cells completely abrogated the antitumor effect of PD-1 blockade in the MC38 model but only had a partial effect in the YUMM2.1 model, whereas CD4 depletion completely reversed the antitumor effect in both models. Considering that anti–PD-1 also controls key T-cell inhibitory interactions between PD-L1 on APCs and PD-1 on T cells (17, 42) and that PD-1 limits CD4 T-cell clonal expansion in response to an immunogenic stimulus (43), it is not surprising that CD4 T cells are required for anti–PD-1/PD-L1 tumor response. However, another group has reported opposite observations, with increased antitumor effect seen with CD4 cell depletion combined with PD-1/PD-L1 blockade (44). Of note, none of the tumor models evaluated by this group was responsive to anti–PD-1/PD-L1 itself. The authors suggested that CD4 cell depletion effect was partially attributed to a removal of CD4-positive immunosuppressive T_{regs}. However, in another report (31), T_{regs} increased after very early analysis (48 and 72 hours) following treatment with anti–PD-1 in MC38, whereas in our tumor models, T_{regs} did not change with anti–PD-1 when analyzed at 10 days after starting therapy.

Next, we characterized anti–PD-1 modulation of the cellular components in the tumor microenvironment. CD8 T cells were expected to increase in both anti–PD-1-responsive tumors. This was true for MC38, but in YUMM2.1, CD8 T cells decreased over time with anti–PD-1 therapy, implying that CD8 T cells may have an early role in this antitumor response. Therefore, the early activation of CD8 T cells could take place during antigen presentation to naïve T cells, where PD-1/PD-L1 costimulation has been shown to lead to T-cell receptor (TCR) downmodulation (16, 17, 42). DCs have been reported to hyperactivate CD8 T cells in the absence of PD-1/PD-L1 costimulation, which was accompanied by a higher TCR surface level and an increase in IFNγ (17). Depending on where PD-1/PD-L1 blockade takes place, T-cell activity may vary. It is unknown if the location of PD-1/PD-L1 interaction and its consecutive blockade is tumor-dependent in a short-term implanted tumor model. Functional studies to determine T-cell activity shortly after anti–PD-1 are administered, and further characterization of the specific CD8 T-cell phenotype could provide some explanation on how CD8 T cells exhibit their effect in this tumor model. The role of natural killer (NK) cells in this setting is unknown and technically challenging because of their low frequency in the tumor microenvironment, but certainly interesting to explore. Differences in PD-1 expression on the CD8 T cells could also be informative to address PD-1 responsiveness in the YUMM2.1 tumor model, as shown by others (31).

The correlation between tumor-intrinsic stabilized β-catenin and both T-cell exclusion and anti–PD-L1 resistance in genetically engineered mice with $BRAF^{V600E}$/$PTEN^{-/-}$/β-catenin–stabilized tumors (34) led us to investigate the effect of β-catenin downregulation in T-cell modulation and anti–PD-1 antitumor response. Although our analysis indicated that YUMM2.1 did not have recombined β-catenin allele that would render β-catenin

more stable, it does have more β-catenin expression and activity compared with the other YUMM cell lines. We observed that T cells were reduced over time (but never upfront excluded) with anti–PD-1 therapy, and this phenomenon was independent from the β-catenin status. PD-1 blockade antitumor effect was not altered in the presence of a downregulated Wnt/β-catenin pathway.

Looking further into the importance of costimulatory interactions during antigen presentation to naïve T cells, we demonstrated that the absence of CD28 or CD80/86 prevented the anti–PD-1 effects in YUMM2.1 tumors. This observation does not necessarily imply that the PD-1/PD-L1 inhibitory effects only take place at the APC–T-cell synapse, but suggest that PD-L1–expressing APCs are positively enhanced upon PD-1 blockade. Indeed, the priming of CD4 and CD8 T cells is more effective in the absence of PD-1/PD-L1 signaling (45), and downmodulation of PD-L1 in DCs results in increased costimulatory molecule CD80 expression and a distinct cytokine profile (46). The same group observed strong tumor growth control when using PD-L1–silenced DCs in a mouse model of lymphoma, although with no increased cure rates, possibly due to PD-L1–expressing tumor cells that might counteract CD8 T-cell activity (47).

Analysis of the different DC subsets in YUMM2.1 tumors revealed an increase in $CD11c^{+}CD11b^{+}MHC-II^{high}$ DCs upon PD-1 blockade, which was not present in the other tumor models analyzed. Cross-priming of tumor antigens by BATF3-dependent DCs is crucial to the efficacy of anti–PD-1 antibodies (48). Taken together, these data imply that priming via CD4 T cells has a more important role in the antitumor efficacy of PD-1 blockade in the YUMM2.1 model.

When looking into the ability of the models to evoke an inflammatory reaction required for immune cell recruitment and DC–T-cell costimulation, YUMM2.1 exhibited an "inflammatory profile" consistent with an endogenous upregulation of immune, cytokine producing, and inflammatory response-related genes. The YUMM2.1 model could therefore intrinsically harbor inflammatory mediators necessary to couple innate recognition to T-cell–mediated immunity by DCs *in vivo*, which is also supported by the increase in chemotactic factors such as Cxcl10, Ccl6, or Cxcl12. This observation is consistent with other reports, where chemokine-trafficking of immune cells into tumors was observed in human melanoma cell lines (49) or in mice receiving adoptive cell therapy and anti–PD-1 blockade (50).

In conclusion, T-cell priming supports anti–PD-1 antitumor responses mediated by CD4 and CD8 T cells, critically requiring costimulation *in vivo*.

Disclosure of Potential Conflicts of Interest

Authors' Contributions

Conception and design: B. Homet Moreno, A. Garcia-Diaz, S. Hu-Lieskovan, A. Ribas
Development of methodology: B. Homet Moreno, A. Garcia-Diaz, M. Bosenberg, B. Comin-Anduix, S. Hu-Lieskovan, A. Ribas
Acquisition of data (provided animals, acquired and managed patients, provided facilities, etc.): B. Homet Moreno, L. Robert, K. Meeth, A.T. Weeraratna, S. Hu-Lieskovan, A. Ribas
Analysis and interpretation of data (e.g., statistical analysis, biostatistics, computational analysis): B. Homet Moreno, J.M. Zaretsky, J. Tsoi, M. Bosenberg, A.T. Weeraratna, T.G. Graeber, B. Comin-Anduix, S. Hu-Lieskovan, A. Ribas

References

620 Q16

622 1. Brahmer JR, Tykodi SS, Chow LQ, Hwu WJ, Topalian SL, Hwu P, et al. Safety
623   and activity of anti–PD-L1 antibody in patients with advanced cancer.
624   N Engl J Med 2012;366:2455–65.
625 2. Hamid O, Robert C, Daud A, Hodi FS, Hwu WJ, Kefford R, et al. Safety and
626   tumor responses with lambrolizumab (anti–PD-1) in melanoma. N Engl
627   J Med 2013;369:134–44.
628 3. Ribas A, Schnachter J, V. Long G, Arance A, Grob JJ, Mortier L, et al. Phase III
629   study of prembrolizumab (MK-3475) versus ipilimumab in patients with
630   ipilimumab-naive advanced melanoma (abstract CT101). Am Assoc Can-
631 Q17   cer Res (Anual Meeting) 2015.
632 4. Topalian SL, Hodi FS, Brahmer JR, Gettinger SN, Smith DC, McDermott DF,
633   et al. Safety, activity, and immune correlates of anti–PD-1 antibody in
634   cancer. N Engl J Med 2012;366:2443–54.
635 5. Taube JM, Klein A, Brahmer JR, Xu H, Pan X, Kim JH, et al. Association of
636   PD-1, PD-1 ligands, and other features of the tumor immune microenvi-
637   ronment with response to anti–PD-1 therapy. Clin Cancer Res 2014;20:
638   5064–74.
639 6. Tumeh PC, Harview CL, Yearley JH, Shintaku IP, Taylor EJ, Robert L, et al.
640   PD-1 blockade induces responses by inhibiting adaptive immune resis-
641   tance. Nature 2014;515:568–71.
642 7. Gubin MM, Zhang X, Schuster H, Caron E, Ward JP, Noguchi T, et al.
643   Checkpoint blockade cancer immunotherapy targets tumour-specific
644   mutant antigens. Nature 2014;515:577–81.
645 8. Blank C, Kuball J, Voelkl S, Wiendl H, Becker B, Walter B, et al. Blockade of
646   PD-L1 (B7-H1) augments human tumor-specific T cell responses in vitro.
647   Int J Cancer 2006;119:317–27.
648 9. Freeman GJ, Long AJ, Iwai Y, Bourque K, Chernova T, Nishimura H, et al.
649   Engagement of the PD-1 immunoinhibitory receptor by a novel B7 family
650   member leads to negative regulation of lymphocyte activation. J Exp Med
651   2000;192:1027–34.
652 10. Latchman YE, Liang SC, Wu Y, Chernova T, Sobel RA, Klemm M, et al. PD-
653   L1-deficient mice show that PD-L1 on T cells, antigen-presenting cells, and
654   host tissues negatively regulates T cells. Proc Natl Acad Sci U S A
655   2004;101:10691–6.
656 11. Wang L, Pino-Lagos K, de Vries VC, Guleria I, Sayegh MH, Noelle RJ.
657   Programmed death 1 ligand signaling regulates the generation of adaptive
658   Foxp3+CD4+ regulatory T cells. Proc Natl Acad Sci U S A 2008;105:
659   9331–6.
660 12. Robert C, Long GV, Brady B, Dutriaux C, Maio M, Mortier L, et al.
661   Nivolumab in previously untreated melanoma without BRAF mutation.
662   N Engl J Med 2015;372:320–30.
663 13. Gilchrest BA, Eller MS, Geller AC, Yaar M. The pathogenesis of melanoma
664   induced by ultraviolet radiation. N Engl J Med 1999;340:1341–8.
665 14. Hecht SS. Tobacco smoke carcinogens and lung cancer. J Natl Cancer Inst
666   1999;91:1194–210.
667 15. Carter L, Fouser LA, Jussif J, Fitz L, Deng B, Wood CR, et al. PD-1:PD-L
668   inhibitory pathway affects both CD4(+) and CD8(+) T cells and is
669   overcome by IL-2. Eur J Immunol 2002;32:634–43.
670 16. Karwacz K, Arce F, Bricogne C, Kochan G, Escors D. PD-L1 co-stimulation,
671   ligand-induced TCR down-modulation and anti-tumor immunotherapy.
672   Oncoimmunology 2012;1:86–8.

17. Karwacz K, Bricogne C, MacDonald D, Arce F, Bennett CL, Collins M, et al.   674
    PD-L1 co-stimulation contributes to ligand-induced T cell receptor down-   675
    modulation on CD8+ T cells. EMBO Mol Med 2011;3:581–92.   676
18. Yokosuka T, Takamatsu M, Kobayashi-Imanishi W, Hashimoto-Tane A,   677
    Azuma M, Saito T. Programmed cell death 1 forms negative costimulatory   678
    microclusters that directly inhibit T cell receptor signaling by recruiting 679
    phosphatase SHP2. J Exp Med 2012;209:1201–17.   680
19. Harada N, Tamai Y, Ishikawa T, Sauer B, Takaku K, Oshima M, et al.   681
    Intestinal polyposis in mice with a dominant stable mutation of the beta-   682
    catenin gene. EMBO J 1999;18:5931–42.   683
20. McKenna A, Hanna M, Banks E, Sivachenko A, Cibulskis K, Kernytsky A,   684
    et al. The Genome Analysis Toolkit: A MapReduce framework for analyzing   685
    next-generation DNA sequencing data. Genome Res 2010;20:1297–303.   686
21. Shi H, Hugo W, Kong X, Hong A, Koya RC, Moriceau G, et al. Acquired   687
    resistance and clonal evolution in melanoma during BRAF inhibitor   688
    therapy. Cancer Discov 2014;4:80–93.   689
22. Koboldt DC, Zhang Q, Larson DE, Shen D, McLellan MD, Lin L, et al.   690
    VarScan 2: Somatic mutation and copy number alteration discovery in   691
    cancer by exome sequencing. Genome Res 2012;22:568–76.   692
23. McLaren W, Pritchard B, Rios D, Chen Y, Flicek P, Cunningham F. Deriving   693
    the consequences of genomic variants with the Ensembl API and SNP Effect   694
    Predictor. Bioinformatics 2010;26:2069–70.   695
24. Favero F, Joshi T, Marquard AM, Birkbak NJ, Krzystanek M, Li Q, et al.   696
    Sequenza: Allele-specific copy number and mutation profiles from tumor   697
    sequencing data. Ann Oncol 2015;26:64–70.   698
25. Kim D, Pertea G, Trapnell C, Pimentel H, Kelley R, Salzberg SL. TopHat2:   699
    accurate alignment of transcriptomes in the presence of insertions, dele-   700
    tions and gene fusions. Genome Biol 2013;14:R36.   701
26. Trapnell C, Roberts A, Goff L, Pertea G, Kim D, Kelley DR, et al. Differential 702
    gene and transcript expression analysis of RNA-seq experiments with   703
    TopHat and Cufflinks. Nat Protoc 2012;7:562–78.   704
27. Subramanian A, Tamayo P, Mootha VK, Mukherjee S, Ebert BL, Gillette MA,   705
    et al. Gene set enrichment analysis: A knowledge-based approach for   706
    interpreting genome-wide expression profiles. Proc Natl Acad Sci U S A   707
    2005;102:15545–50.   708
28. Cooper ZA, Juneja VR, Sage PT, Frederick DT, Piris A, Mitra D, et al.   709
    Response to BRAF inhibition in melanoma is enhanced when combined   710
    with immune checkpoint blockade. Cancer Immunol Res 2014;2:643–54.   711
29. Koya RC, Mok S, Comin-Anduix B, Chodon T, Radu CG, Nishimura MI,   712
    et al. Kinetic phases of distribution and tumor targeting by T cell receptor 713
    engineered lymphocytes inducing robust antitumor responses. Proc Natl   714
    Acad Sci U S A 2010;107:14286–91.   715
30. Cross RS, Malaterre J, Davenport AJ, Carpinteri S, Anderson RL, Darcy PK,   716
    et al. Therapeutic DNA vaccination against colorectal cancer by targeting   717
    the MYB oncoprotein. Clin Transl Immunol 2015;4:e30.   718
31. Ngiow SF, Young A, Jacquelot N, Yamazaki T, Enot D, Zitvogel L, et al. A   719
    threshold level of intratumor CD8+ T-cell PD1 expression dictates ther-   720
    apeutic response to anti-PD1. Cancer Res 2015;75:3800–11.   721
32. Mule JJ, Shu S, Schwarz SL, Rosenberg SA. Adoptive immunotherapy of   722
    established pulmonary metastases with LAK cells and recombinant inter-   723
    leukin-2. Science 1984;225:1487–9.   724

33. Damsky WE, Curley DP, Santhanakrishnan M, Rosenbaum LE, Platt JT, Gould Rothberg BE, et al. Beta-catenin signaling controls metastasis in Braf-activated Pten-deficient melanomas. Cancer Cell 2011;20:741–54.

34. Spranger S, Bao R, Gajewski TF. Melanoma-intrinsic beta-catenin signalling prevents anti-tumour immunity. Nature 2015;523:231–5.

35. Ginhoux F, Liu K, Helft J, Bogunovic M, Greter M, Hashimoto D, et al. The origin and development of nonlymphoid tissue CD103+ DCs. J Exp Med 2009;206:3115–30.

36. Ganguly D, Haak S, Sisirak V, Reizis B. The role of dendritic cells in autoimmunity. Nat Rev Immunol 2013;13:566–77.

37. Ribas A. Adaptive immune resistance: How cancer protects from immune attack. Cancer Discov 2015;5:915–9.

38. Snyder A, Makarov V, Merghoub T, Yuan J, Zaretsky JM, Desrichard A, et al. Genetic basis for clinical response to CTLA-4 blockade in melanoma. N Engl J Med 2014;371:2189–99.

39. Rizvi NA, Hellmann MD, Snyder A, Kvistborg P, Makarov V, Havel JJ, et al. Cancer immunology. Mutational landscape determines sensitivity to PD-1 blockade in non-small cell lung cancer. Science 2015;348:124–8.

40. Le DT, Uram JN, Wang H, Bartlett BR, Kemberling H, Eyring AD, et al. PD-1 blockade in tumors with mismatch-repair deficiency. N Engl J Med 2015;372:2509–20.

41. Hirano F, Kaneko K, Tamura H, Dong H, Wang S, Ichikawa M, et al. Blockade of B7-H1 and PD-1 by monoclonal antibodies potentiates cancer therapeutic immunity. Cancer Res 2005;65:1089–96.

42. Escors D, Bricogne C, Arce F, Kochan G, Karwacz K. On the mechanism of T cell receptor down-modulation and its physiological significance. J Biosci Med 2011;1.

43. Konkel JE, Frommer F, Leech MD, Yagita H, Waisman A, Anderton SM. PD-1 signalling in CD4(+) T cells restrains their clonal expansion to an immunogenic stimulus, but is not critically required for peptide-induced tolerance. Immunology 2010;130:92–102.

44. Ueha S, Yokochi S, Ishiwata Y, Ogiwara H, Chand K, Nakajima T, et al. Robust antitumor effects of combined anti-CD4-depleting antibody and anti-PD-1/PD-L1 immune checkpoint antibody treatment in mice. Cancer Immunol Res 2015;3:631–40.

45. Gibson A, Ogese M, Sullivan A, Wang E, Saide K, Whitaker P, et al. Negative regulation by PD-L1 during drug-specific priming of IL-22-secreting T cells and the influence of PD-1 on effector T cell function. J Immunol 2014;192:2611–21.

46. Pen JJ, Keersmaecker BD, Heirman C, Corthals J, Liechtenstein T, Escors D, et al. Interference with PD-L1/PD-1 co-stimulation during antigen presentation enhances the multifunctionality of antigen-specific T cells. Gene Ther 2014;21:262–71.

47. Blank C, Gajewski TF, Mackensen A. Interaction of PD-L1 on tumor cells with PD-1 on tumor-specific T cells as a mechanism of immune evasion: Implications for tumor immunotherapy. Cancer Immunol Immunother 2005;54:307–14.

48. Sanchez-Paulete AR, Cueto FJ, Martinez-Lopez M, Labiano S, Morales-Kastresana A, Rodriguez-Ruiz ME, et al. Cancer immunotherapy with immunomodulatory anti-CD137 and anti-PD-1 monoclonal antibodies requires BATF3-dependent dendritic cells. Cancer Discov 2016;6:71–9.

49. Harlin H, Meng Y, Peterson AC, Zha Y, Tretiakova M, Slingluff C, et al. Chemokine expression in melanoma metastases associated with CD8+ T-cell recruitment. Cancer Res 2009;69:3077–85.

50. Peng W, Liu C, Xu C, Lou Y, Chen J, Yang Y, et al. PD-1 blockade enhances T-cell migration to tumors by elevating IFN-gamma inducible chemokines. Cancer Res 2012;72:5209–18.

AUTHOR QUERIES

AUTHOR PLEASE ANSWER ALL QUERIES

Q1: Page: 1: AU: Per journal style, genes, alleles, loci, and oncogenes are italicized; proteins are roman. Please check throughout to see that the words are styled correctly. AACR journals have developed explicit instructions about reporting results from experiments involving the use of animal models as well as the use of approved gene and protein nomenclature at their first mention in the manuscript. Please review the instructions at http://www.aacrjournals.org/site/InstrAuthors/ifora.xhtml#genenomen to ensure that your article is in compliance. If your article is not in compliance, please make the appropriate changes in your proof.

Q2: Page: 1: Author: Please verify the drug names and their dosages used in the article.

Q3: Page: 1: Author: Please check the affiliation addresses as set for correctness.

Q4: Page: 1: Author: Please verify the affiliations and their corresponding author links.

Q5: Page: 1: Author: Please verify the corresponding author details.

Q6: Page: 2: Author: Please define "AALAC."

Q7: Page: 2: Author: Units of measurement have been changed here and elsewhere in the text from "M" to "mol/L," and related units, such as "mmol/L" and "μmol/L," in figures, legends, and tables in accordance with journal style, derived from the Council of Science Editors Manual for Authors, Editors, and Publishers and the Système international d'unités. Please note if these changes are not acceptable or appropriate in this instance.

Q8: Page: 2: Author: Please check "ratio.priority" for sense.

Q9: Page: 2: Author: Please define "OCT."

Q10: Page: 3: Author: Please confirm quality/labeling of all images included within this article. Thank you.

Q11: Page: 6: Author: Please verify the reference to "2C" in the part "analysis of the 2C total number" for sense.

Q12: Page: 6: Author: Please define "APCs."

Q13: Page: 11: AU:/PE: The conflict-of-interest disclosure statement that appears in the proof incorporates the information from forms completed and signed off on by each individual author. No factual changes can be made to disclosure information at the proof stage. However, typographical errors or misspelling of author names should be noted on the proof and will be corrected before publication. Please note if any such errors need to be corrected. Is the disclosure statement correct?

Q14: Page: 12: Author: The contribution(s) of each author are listed in the proof under the heading "Authors' Contributions." These contributions are derived from forms completed and signed off on by each individual author. As the corresponding author, you are

permitted to make changes to your own contributions. However, because all authors submit their contributions individually, you are not permitted to make changes in the contributions listed for any other authors. If you feel strongly that an error is being made, then you may ask the author or authors in question to contact us about making the changes. Please note, however, that the manuscript would be held from further processing until this issue is resolved.

Q15: Page: 12: Author: Please verify the heading "Grant Support" and its content for correctness.

Q16: Page: 12: Author: Ref. 37 has been updated as per PubMed. Please verify.

Q17: Page: 12: Author: Please provide volume and page range for ref. 3.

AU: Below is a summary of the name segmentation for the authors according to our records. The First Name and the Surname data will be provided to PubMed when the article is indexed for searching. Please check each name carefully and verify that the First Name and Surname are correct. If a name is not segmented correctly, please write the correct First Name and Surname on this page and return it with your proofs. If no changes are made to this list, we will assume that the names are segmented correctly, and the names will be indexed as is by PubMed and other indexing services.

First Name	Surname
		Antoni	Ribas
Blanca	
Homet Moreno	
Jesse M.	Zaretsky
Angel	Garcia-Diaz
Jennifer	Tsoi
Giulia	Parisi
Lidia	Robert
Katrina	Meeth
Abibatou	Ndoye
Marcus	Bosenberg
Ashani T.	Weeraratna
Thomas G.	Graeber
Begoña	Comin-Anduix
Siwen	Hu-Lieskovan